Hindawi
Geofluids
Volume 2019, Article ID 3729381, 14 pages
https://doi.org/10.1155/2019/3729381

Research Article

Investigation of the Velocities of Coals of Diverse Rank under Water- or Gas-Saturated Conditions for Application in Coalbed Methane Recovery

Jizhao Xu,[1,2,3,4] Cheng Zhai,[1,2,3] Pathegama Gamage Ranjith,[4] Yong Sun,[1,2,3] Jisheng Guo,[1,2,3] Zheng Ma,[1,2,3] Huiteng Ma,[1,2,3] and Lei Qin[5]

[1]*Key Laboratory of Coal Methane and Fire Control, Ministry of Education, China University of Mining and Technology, Xuzhou, Jiangsu 221116, China*
[2]*State Key Laboratory of Coal Resources and Safe Mining, Xuzhou, Jiangsu 221116, China*
[3]*School of Safety Engineering, China University of Mining and Technology, 221116 Xuzhou, China*
[4]*Department of Civil Engineering, Building 60, Monash University, Clayton, VIC 3800, Australia*
[5]*College of Safety Science and Engineering, Xi'an University of Science and Technology, 710054 Xi'an, China*

Correspondence should be addressed to Cheng Zhai; greatzc@cumt.edu.cn

Received 30 November 2018; Revised 29 January 2019; Accepted 27 March 2019; Published 2 May 2019

Guest Editor: Giorgio Minelli

Coalbed methane recovery enhanced by hydraulic or nonaqueous fracturing methods has been studied for decades, and it is of significance to evaluate fracturing results and scope for field applications. Monitoring variation in velocity is one way to explain fracturing effects. However, the existence of residual water or gas within cracks or pores may affect velocity measurements, and the correlation between velocity and inherent coal attributes (such as density and porosity) has not been studied comprehensively. In this paper, coal of different ranks (lignite, bituminite, and anthracite) was prepared under water and gas saturation to approximately simulate the residual water and gas in cracks under field applications. Correlations between the velocity and coal attributes were studied. For both water- and gas-saturated cores, the diverse velocity distributions were highly correlated to rank and saturation media. The longitudinal ultrasonic pulse velocity (UPVp) and transverse ultrasonic pulse velocity (UPVs) of different cores were distributed differently. For coal saturated with water or gas, the UPVp values of lignite, bituminite, and anthracite had positive linear correlations with the corresponding UPVs values. The discrete velocity ratio data were fit as negative linear correlations with UPVs, and different coals had different declining degrees, the difference of which might be attributed to the characteristics of structural cracks and the inherent properties of the coal, such as grain size and pore shape, which result in decreasing coal integrity and strength. Moreover, the difference in acoustic resistance between coal and fluids might have an inverse impact on the acoustic energy, and a larger difference might cause a large amount of energy to dissipate and finally cause the velocity to decrease. Under water and gas saturation conditions, the UPVp showed a positive linear correlation with density and a negative linear correlation with porosity. Finally, a potential field application was designed on the relations between the velocity and the elastic parameters to estimate fracturing effects by monitoring the petrophysical parameters of coal lithologies.

1. Introduction

Effective coalbed methane (CBM) drainage is a topical research issue around the world. CBM also occupies an increasing proportion of the resource structure in China, and its efficient use is likely to ease the pressure on other diminishing fossil fuel reserves [1–4]. CBM reserves in China typically have properties that constrain their extractability, such as great depth, great density, or low permeability [5–7]. Some technologies, such as hydraulic and nonaqueous fracturing, have been proposed to improve fracture connection and thus enhance the permeability of the CBM reserves

[8–11]. Meanwhile, the inherent properties of coal also play an important role in controlling fracturing [12–14]. For example, bulk density and strength (bulk modulus and shear modulus) provide information about integrity under different pressure-temperature states, as well as mineral constituents and their distribution influence homogeneity. Coal rank correlates with the degree of anisotropy in some respects, such as anisotropic ultrasonic velocity, porosity, and fracture orientation. It is of significance to evaluate fracturing results and scope for field applications. The ultrasonic pulse velocity (UPV) method is commonly used to obtain various information on material properties and rock quality because it is convenient, nondestructive, and highly efficient [15, 16]. The UPV method can be used to detect microscopic cracks within the matrix [17, 18] and to evaluate the efficacy of consolidation in concrete [19, 20].

The UPV testing method in a laboratory setting uses a pair of transducers (one transducer as a signal emitter and another transducer as a receiver) to quantify ultrasonic pulse transmission through a sample using an oscilloscope. There are two main parameters of interest: longitudinal ultrasonic pulse velocity (UPVp) and transverse ultrasonic pulse velocity (UPVs), as shown in Figure 1. The velocity is calculated as follows [21]:

$$V = \frac{L}{t_2 - t_1}, \tag{1}$$

where L is the length of the sample, t_1 and t_2 are the docking time of the transducers and the first arrival time of the wave signal by the receiver sensor, respectively, and $t_2 - t_1$ is the travel time.

Vilhelm et al. [22] studied velocity dispersion in fractured rocks over a wide frequency range (~1 kHz, ~40 kHz, and ~1 MHz) and successfully used a displacement discontinuity approach in a theoretical model to conclude that the first arrivals of seismic waves can be used to evaluate *P*-wave velocity. Nakahata et al. [23] proposed a time domain simulation tool based on finite integration and an image-based modeling approach to better understand the characteristics of ultrasonic wave propagation in concrete. Pulse wave velocities are thought to reflect the mechanical properties of rocks [24–27], which were evaluated using the UPV method by Vasanelli et al. [28], in terms of the physical and mechanical properties of a highly porous building limestone. Statistical information on the correlation between compressional and shear wave velocities and the corresponding Poisson's ratios of different lithologies at different pressure-temperature conditions has also been found [29–33]. Lokajíček et al. [34] studied the influence of thermal heating on elastic wave velocity within granulite samples under different stress levels using a three-dimensional *P*-wave elastic anisotropy method.

UPV testing has also been used to evaluate coal properties and various influencing factors such as confining stress, temperature, moisture content, and porosity. The ultrasonic wave velocity of coal under lower confining stress increases with rank because of fracture closure [35, 36]. Liu et al. [37] divided the effects of water saturation on *P*-wave propagation in fractured coal into three types. Pulse wave velocity and anisotropy of tectonically deformed coal have been used to show that the Vp/Vs ratio, Poisson's ratio, and anisotropy are all sensitive to deformation type and extent [21]. Additionally, structural fractures were found to have a significant impact on the elastic properties of coal samples from different deformation environments [21]. Lwin [38] studied the effect of different gases (He, N_2, CH_4, and CO_2) on the ultrasonic response of coal and revealed a significant difference in density, *P*-wave modulus, and impedance for CO_2 saturation compared with CH_4 saturation. Yu et al. [39] studied pore variations and changes in *P*-wave velocity of coal affected by ultrasonic excitation and found that the *P*-wave velocity decreased with increasingly affected cycles.

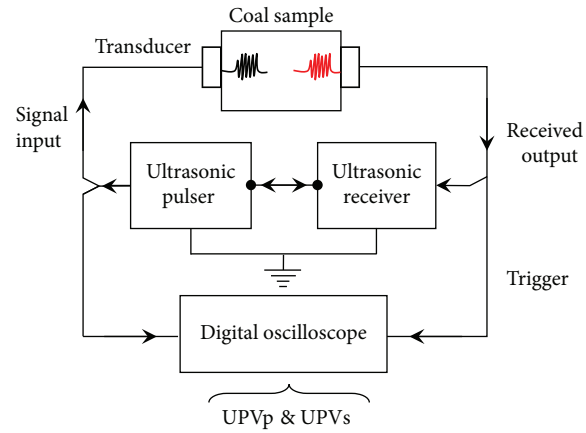

Figure 1: Schematic diagram of the UPV device used in this study.

The velocity monitoring method has been applied to fracturing estimation; however, residual water or gas occupies pores and cracks after fracturing. The impact of residual water or gas on the accurate evaluation of velocity and the correlations between inherent attributes (porosity, density, and rank) have not been studied comprehensively. In this paper, three different ranks of coals, including 24 lignites, 26 bituminites, and 26 anthracites, are tested (UPVp and UPVs) under both water and gas (air) saturation. The correlations among velocity, density, and porosity are described, and the statistical results can provide reference parameters for further field monitoring in coal physics in terms of CBM reservoir fracturing processes.

2. Materials and Methods

2.1. Coal Preparation. Lignite, bituminite, and anthracite samples were collected from the Shengli Coal Mine, Inner Mongolia; the Datong Coal Mine, Shanxi; and the Yangzhuang Coal Mine, Huaibei; respectively. The large coal blocks were wrapped with preservative film and transferred to the State Key Laboratory of Coal Resources and Safe Mining in Xuzhou, Jiangsu, before being cored to produce 5 cm diameter cylinders with 10 cm height (Figures 2(a) and 2(b)). To conveniently measure the pulse velocity of the cores, the tops and bottoms of the cylinders were ground flat to ensure a parallelism error of ≤0.005 mm [40]. The detailed properties of the 24 lignite cores ($R_{o,max}$ of 0.32), 26 bituminite cores

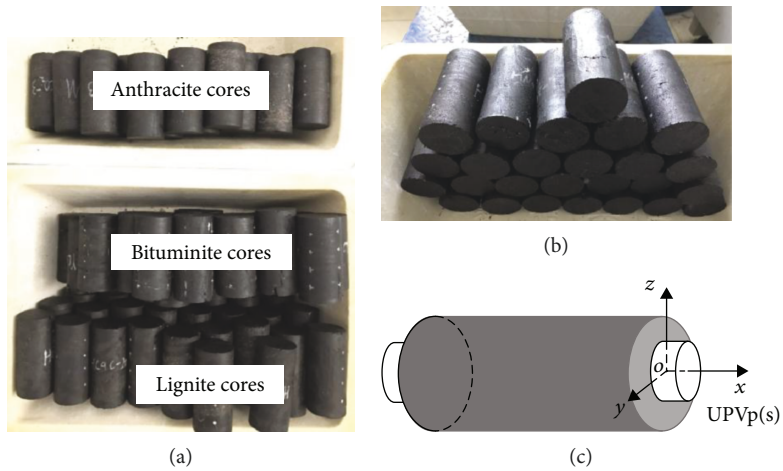

FIGURE 2: Images of 76 coals with different ranks. (a) Overall view of the 76 coal cores, (b) lateral display of lignite cores, and (c) sketch image of UPV test method.

($R_{o,max}$ of 1.13), and 26 anthracite cores ($R_{o,max}$ of 3.05) [41] are listed in Table 1. The density of the lignite, bituminite, and anthracite cores was measured to be 1.28 g/cm^3 to 1.55 g/cm^3, 1.23 g/cm^3 to 1.42 g/cm^3, and 1.29 g/cm^3 to 1.61 g/cm^3, respectively. The porosity of the cores was measured to be in the ranges of 1.07% to 3.17%, 0.3% to 4.0% and 0.3% to 2.9%, respectively. The core samples were preserved in a curing box to maintain their original structure and moisture content.

2.2. Experimental Equipment and Procedures. The UPV test equipment used to record the UPVp and UPVs values of the cores under water and gas saturation (the gas during the experiment and referred to in the paper is air) was an HS-YS4A Sonic wave parameter tester (Tianhong Electronics, Xiangtan, China). This apparatus operates with a high signal-to-noise ratio and has low temperature excursions and high repeatability with low failure rate. The instrument has two emitter options, 160 V or 1000 V, and the amplifier can be regulated with multistage attenuation processes.

Gas saturation was carried out in an autoclave with a pressure of 1.5 MPa to ensure that air occupied the internal pores or cracks in the cores, and water saturation was undertaken using a vacuum pump (ZN-BSJ, Suzhou Niumag Analytical Instrument Corporation, Suzhou, China) by depressurizing the cores to approximately -1.0 MPa, thus allowing water ingress into the pore spaces of the core.

The ambient temperature during the experiments was 25°C, and to eliminate the high-frequency effect on fluid-saturated samples when measuring velocity, the 160 V emitter was chosen with a frequency of 50 kHz. The experimental procedure was carried out in the following steps:

(i) All the cores were placed in a vacuum drying oven at 60°C for 72 h to remove the original gas and water from the cores, and their masses were tested using an electronic balance and were recorded as M_{pre}

(ii) The cores were placed in the autoclave at a pressure of 1.5 MPa for 72 h to achieve gas saturation, the velocity parameters were tested using the velocity apparatus by connecting the core surface and the transducers, and the values were recorded as $UPVp_{-gas}$ and $UPVs_{-gas}$

(iii) The cores were then immersed in the water saturator, and all the air was exhausted to ensure that water occupied the pores, at a pressure of -0.95 MPa for 72 h. The mass of water-saturated cores was recorded as M_{water}; then, the velocities were measured as $UPVp_{-water}$ and $UPVs_{-water}$

3. Results

Figure 3 shows box plots of velocity recorded in different cores. There are significant differences in terms of velocity distribution and discrete degree according to coal rank and saturation media. For example, the box plot ranges (from lower to upper quartile) of UPVp are larger than those of UPVs for both water-saturated and gas-saturated cores. The UPVp(s) box plot ranges of water-saturated cores exceed those of gas-saturated cores. Water saturation in microcracks improves the continuity of wave propagation with less discrete velocity than gas saturation conditions. Statistically, the width of the UPVp box plots is smaller than the corresponding UPVs box plots under water saturation conditions, which indicates that UPVp has less data dispersion than UPVs. Thus, UPVp is more accurate or reliable for characterizing the existence of micro- or macrocracks with the assistance of adsorbed water. Anthracite cores have a smaller UPVp box plot width than the other plots, which means that the greater rank has less porosity and higher homogeneity, resulting in greater velocity concentration.

UPVp and UPVs velocity ranges and mean values for the three types of coal are listed in Table 2. The largest values in the velocity ranges were recorded in anthracite cores ($UPVp_{-water}$ 1.63 km/s to 2.25 km/s, $UPVs_{-water}$ 1.26 km/s to 1.87 km/s, $UPVp_{-gas}$ 1.12 km/s to 1.94 km/s, and $UPVs_{-gas}$ 0.74 km/s to 1.69 km/s). The lowest velocity ranges were recorded in lignite cores, with intermediate values recorded

Table 1: Detail properties of the coals with different ranks.

Type	Density (g/cm^3)	Porosity (%)	Proximate analysis (%)				$R_{o,max}$ (%)	Maceral analysis (%)			
			M_{ad}	A_{ad}	V_{daf}	FC_{ad}		V	I	E	M
Lignite	1.28-1.55	1.07-3.17	11.37	14.63	53.41	20.59	0.32	79.5	15.5	3.6	1.4
Bituminite	1.23-1.42	0.3-4.0	8.83	3.30	29.64	58.23	1.13	58.7	32.6	3.4	5.3
Anthracite	1.29-1.61	0.3- 2.9	2.10	7.73	6.48	83.69	3.05	86.4	10.5	1.5	1.6

M_{ad}: water content; A_{ad}: ash content; V_{daf}: volatile component; FC_{ad}: fixed carbon content; V: vitrinite; I: inertinite; E: exinite; M: mineral content; $R_{o,max}$: the maximum reflectance of vitrinite.

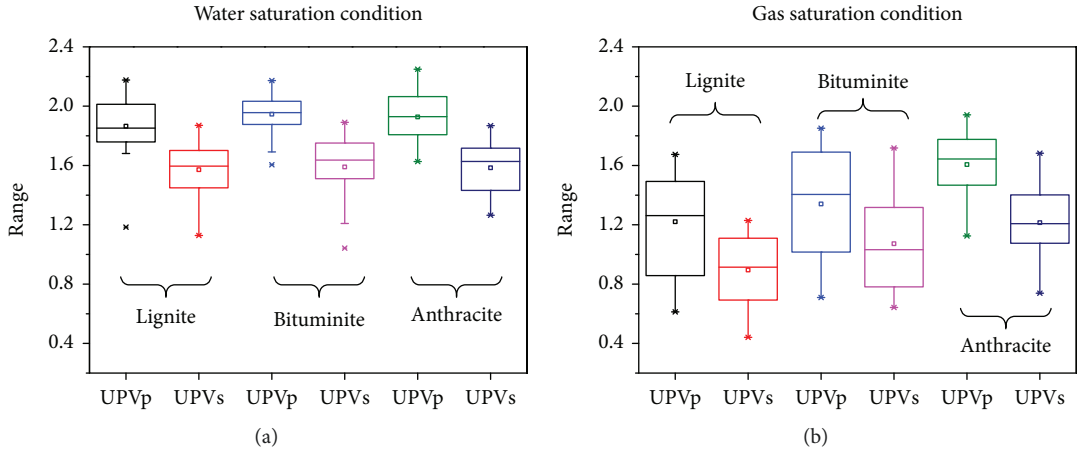

Figure 3: Box plots of different coal rank samples at (a) water saturation and (b) gas saturation condition.

Table 2: UPVp and UPVs velocity ranges and the mean values of three ranks of coals.

	Water saturation condition (km/s)				Gas saturation condition (km/s)			
	UPVp	$UPVp_{mean}$	UPVs	$UPVs_{mean}$	UPVp	$UPVp_{mean}$	UPVs	$UPVs_{mean}$
Lignite	[1.18, 2.17]	1.86	[1.13, 1.87]	1.57	[0.61, 1.67]	1.22	[0.44, 1.23]	0.90
Bituminite	[1.61, 2.17]	1.95	[1.04, 1.89]	1.59	[0.71, 1.85]	1.34	[0.64, 1.72]	1.07
Anthracite	[1.63, 2.25]	1.93	[1.26, 1.87]	1.58	[1.12, 1.94]	1.61	[0.74, 1.69]	1.21

in bituminite cores. In addition, the anthracite cores had the largest $UPVp_{mean}$ value of 1.93 km/s and $UPVs_{mean}$ value of 1.58 km/s under water saturation, with $UPVp_{mean}$ and $UPVs_{mean}$ values of 1.61 km/s and 1.21 km/s, respectively, under gas saturation. The mean velocity values of other sample types followed a trend similar to the measured velocities, and it is posited that coal rank is largely responsible for the variation in recorded ultrasonic velocity.

4. Discussion

4.1. Correlation between UPVp and UPVs. Given the different velocity distributions of the three ranks of coal, it is necessary to analyze correlations between the UPVp and UPVs under the two different conditions. The scatter of velocity data and correlations of fit are shown in Figure 4. The UPVp and UPVs values of the cores differed for both conditions, and they might depend on the coal rank and components within the coal matrix. Velocity values of cores from the same coal blocks were not consistent, because of the various orientations and distributions of microcracks. When an elastic wave transfers to existing defects, such as cleats, cracks, or pores, some reflection, refraction, and diffraction of waves and friction at the crack surface and the grain boundaries might be generated, causing amplitude attenuation and energy decrease [21, 40, 42]. The crack number and distribution might be the main factors influencing velocity decrease. The larger the number of existing cracks is, the greater the energy decrease, and the smaller the velocity is. Under water and gas saturation, the UPVp values generally exceed the UPVs values, and the UPVp and UPVs values of the same cores under water saturation exceed those under gas saturation, indicating that the discrete degree of velocity might occur more frequently under gas saturation due to the large dispersion of air molecules. The scatter in velocity data values is well fit and listed in Table 3.

Dependent on Figure 4, the UPVp values of lignite, bituminite, and anthracite coal showed positive linear correlations

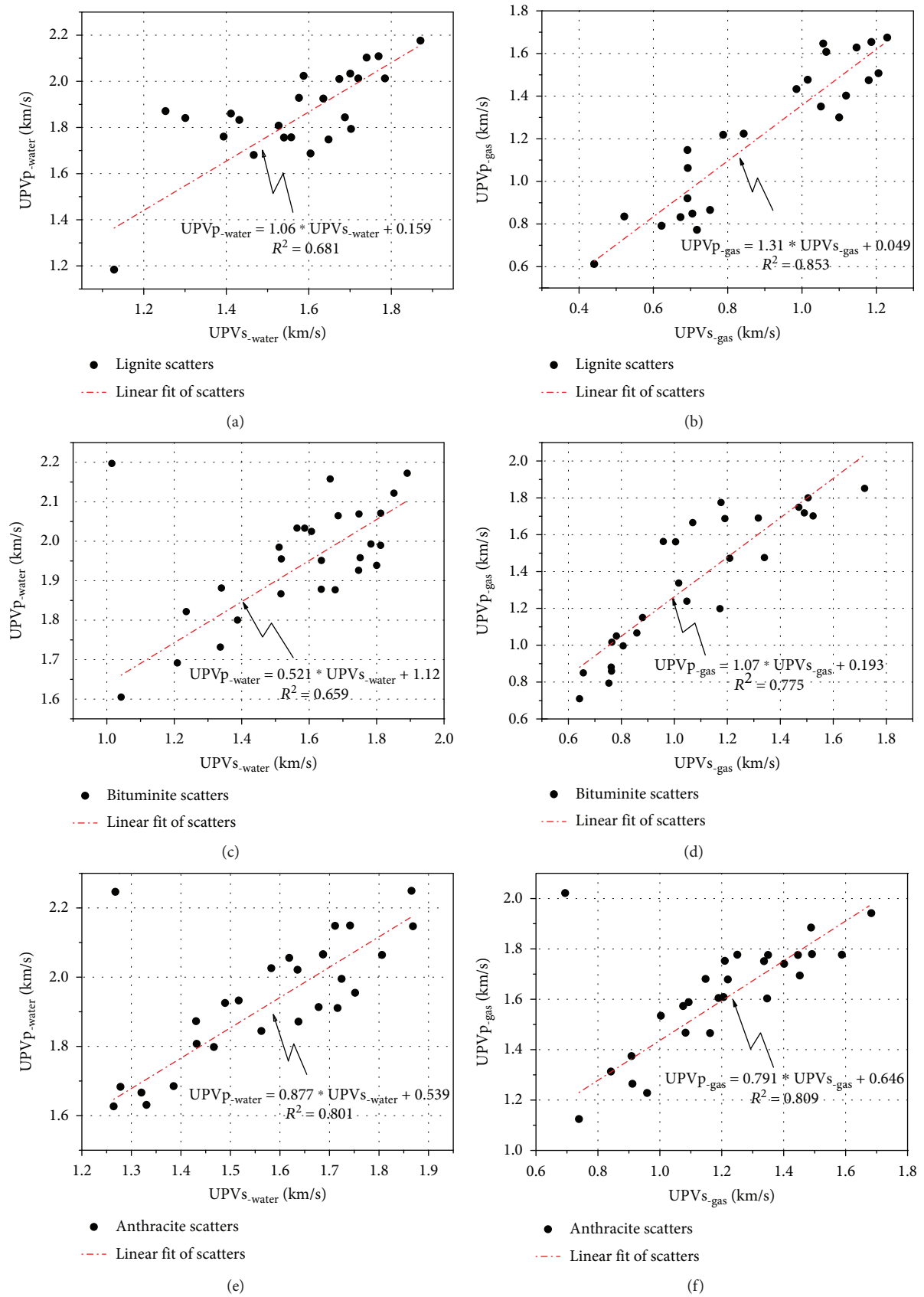

Figure 4: Scatterplot of velocity data and goodness-of-fit correlations between UPVs and UPVp of lignite, bituminite, and anthracite cores under water and gas saturation.

Table 3: Correlations between UPVp and UPVs for lignite, bituminite, and anthracite under water or gas saturation.

	Condition	Equation	R^2
Lignite	Water saturation	$UPVp_{-water} = 1.06^{*}UPVs_{-water} + 0.159$	0.681
	Gas saturation	$UPVp_{-gas} = 1.31^{*}UPVs_{-gas} + 0.049$	0.853
Bituminite	Water saturation	$UPVp_{-water} = 0.521^{*}UPVs_{-water} + 1.12$	0.659
	Gas saturation	$UPVp_{-gas} = 1.07^{*}UPVs_{-gas} + 0.193$	0.775
Anthracite	Water saturation	$UPVp_{-water} = 0.877^{*}UPVs_{-water} + 0.539$	0.801
	Gas saturation	$UPVp_{-gas} = 0.791^{*}UPVs_{-gas} + 0.646$	0.809

with their corresponding UPVs values, under water and gas saturation, similar to the results reported by Kahraman [16], Sayed et al. [43], and Kassab and Weller [44] that UPVp scatter had a strong linear correlation with the corresponding UPVs scatter of dry rock or wet rock samples. When the UPVs-water value was 2.0 km/s, the potential UPVp-water values of lignite, bituminite, and anthracite were 2.279 km/s, 2.162 km/s, and 2.293 km/s, respectively. This difference appears to be dependent on porosity and moisture content, given that the lower the porosity and the higher the moisture content is, the larger the UPVp value is [45].

4.2. Analysis of Velocity Ratio vs. UPVs. Because the different cores have various UPVp and UPVs values, a parameter Vr, namely, velocity ratio, is introduced to eliminate the impact of coal volume and density [21, 37] (seen in equation (2)) and to explore potential correlations between the ratio and the corresponding UPVs values for lignite, bituminite, and anthracite.

$$\begin{cases} Vr_{\text{-water}} = \dfrac{UPVp_{\text{-water}(i)}}{UPVs_{\text{-water}(i)}}, \\ Vr_{\text{-gas}} = \dfrac{UPVp_{\text{-gas}(i)}}{UPVs_{\text{-gas}(i)}}, \end{cases} \tag{2}$$

where Vr_{-water} and Vr_{-gas} are the velocity ratios of coal under water and gas saturation, respectively, and i is the number of one kind of coal; specifically, i equals to 24 for lignite and 26 for bituminite and anthracite. As seen in Figure 5, Vr correlates linearly with the corresponding UPVs values. The linear fitting equations are listed in Table 4. These discrete Vr data are fitted as negative linear relationships with UPVs, and different coals have different declining degrees. The difference in the velocity ratio might be attributed to the characteristics of structural cracks and inherent properties of the coal, such as grain size and pore shape, which result in the decrease of the coal integrity and strength.

For one particular coal with certain porosity, elastic waves show different responses to different fluids occupying the cracks; for example, the UPVp has higher sensitivity with a small amount of gas compared to the UPVs, and the UPVp value might decrease by a larger degree than the UPVs value [46, 47]. As shown in Figure 5, the declining tendency of the correlations between Vr and UPVs indicates that the degree of increase in the UPVp is smaller than that in the UPVs, when the elastic wave propagates via cracks occupied by fluids. According to Kuster and Toksoz [40], different media had different acoustic resistance (AR) values; for example, the AR value of gas was 0.0043×10^4 g/(m^{2*}s), whereas that of water was $(0.29 - 0.66) \times 10^4$ g/(m^{2*}s), and coal had a smaller AR difference with water. It seemed that the difference in declining tendency might be attributed to coal rank, and the coal with a lower rank had a large amount of fissures. When the fissures were filled with water or gas, the larger AR difference between the coal and gas caused a large amount of energy to dissipate by means of wave reflection or refraction, and the Vr value changes were greater. Thus, the existence of cracks or pores had a significant inverse effect on wave velocity, considering the occupying fluids and coal rank.

Moreover, under water saturation conditions, the Vr scatter of lignite, bituminite, and anthracite had good linear fits with the corresponding UPVs, whereas the velocity ratio scatter of lignite and bituminite was more discrete under gas saturation, and those of anthracite had good linear correlation with the UPVs gas. The difference was expected that the adsorbed water improved the matrix homogeneity, given that the density of water exceeds that of air used in the experiments. Lignite had a mean Vr value of 1.19 when water-saturated and 1.36 when gas-saturated. Bituminite and anthracite had mean Vr values of 1.24 and 1.22, respectively, when they were under water saturation, and they had mean values of 1.26 and 1.34, respectively, under gas saturation. According to the linear fitting, when the $UPVs_{\text{-water}}$ value was 1.4 km/s, the potential $Vr_{\text{-water}}$ values of lignite, bituminite, and anthracite were 1.285, 1.335, and 1.259, respectively, and when the $UPVs_{\text{-gas}}$ value was 1.0 km/s, the potential $Vr_{\text{-gas}}$ values of lignite, bituminite, and anthracite were 1.418, 1.239, and 1.443, respectively. The parameter Vr value of coal might provide evidence to locate the cracks after fracturing by measuring the velocity ratio using the measure media.

4.3. Correlations between UPVp and Density. Figure 6 shows the distributions and relationships between UPVp and density for lignite, bituminite, and anthracite cores under water- and gas-saturated conditions, by considering the acoustic signal travel time along the coal sample. There were positive linear correlations between the UPVp and the density for lignite, bituminite, and anthracite under the two

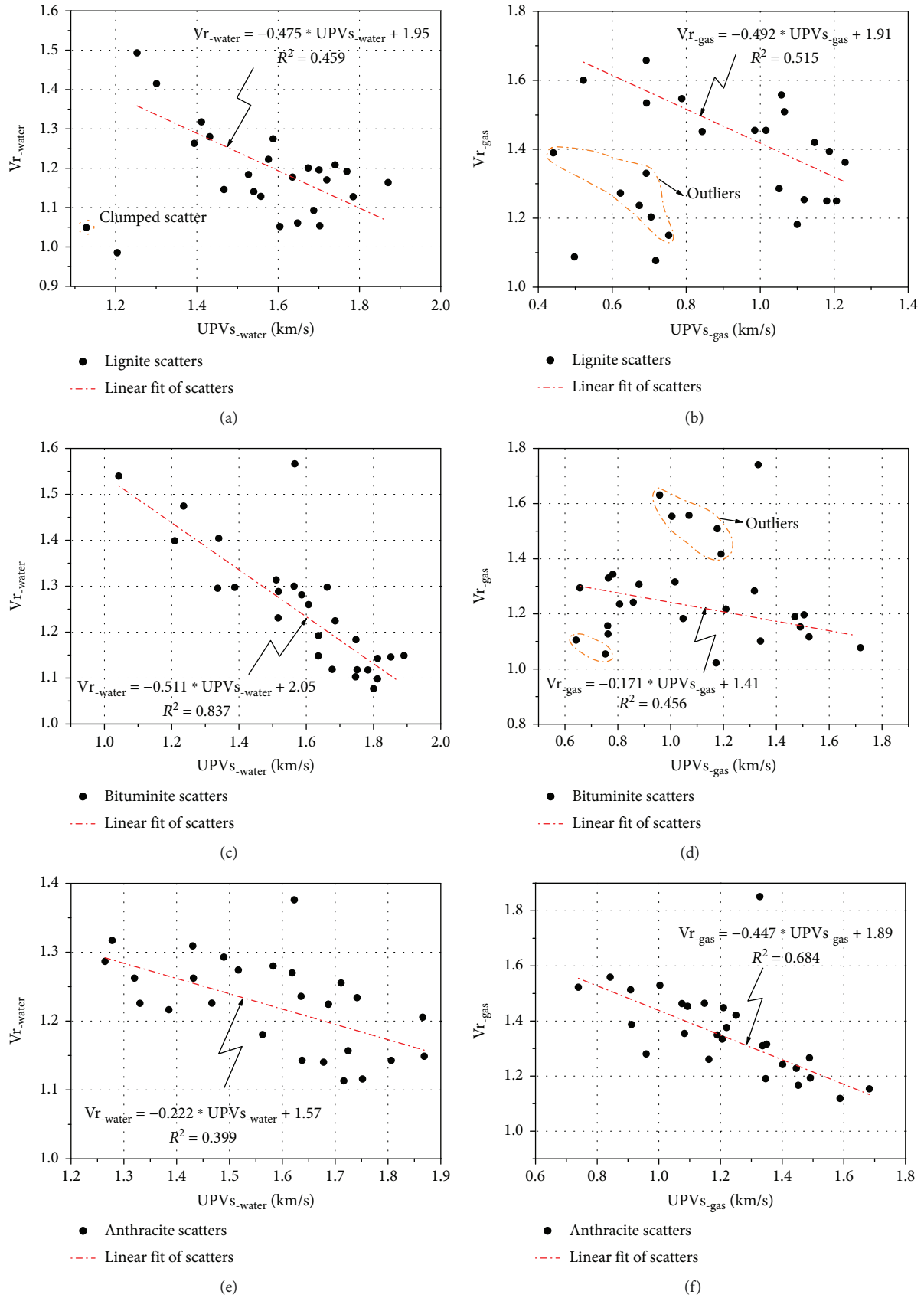

FIGURE 5: Correlations between $Vr_{\text{-water}}$ and $UPVs_{\text{-water}}$ and between $Vr_{\text{-gas}}$ and $UPVs_{\text{-gas}}$ for (a, b) lignite, (c, d) bituminite, and (e, f) anthracite.

Table 4: Linear fit equations of Vr for lignite, bituminite, and anthracite under water and gas saturation.

	Condition	Equation	R^2
Lignite	Water saturation	$Vr_{-water} = -0.475^*UPVs_{-water} + 1.95$	0.459
	Gas saturation	$Vr_{-gas} = -0.492^*UPVs_{-gas} + 1.91$	0.515
Bituminite	Water saturation	$Vr_{-water} = -0.511^*UPVs_{-water} + 2.05$	0.837
	Gas saturation	$Vr_{-gas} = -0.171^*UPVs_{-gas} + 1.41$	0.456
Anthracite	Water saturation	$Vr_{-water} = -0.222^*UPVs_{-water} + 1.57$	0.399
	Gas saturation	$Vr_{-gas} = -0.447^*UPVs_{-gas} + 1.89$	0.684

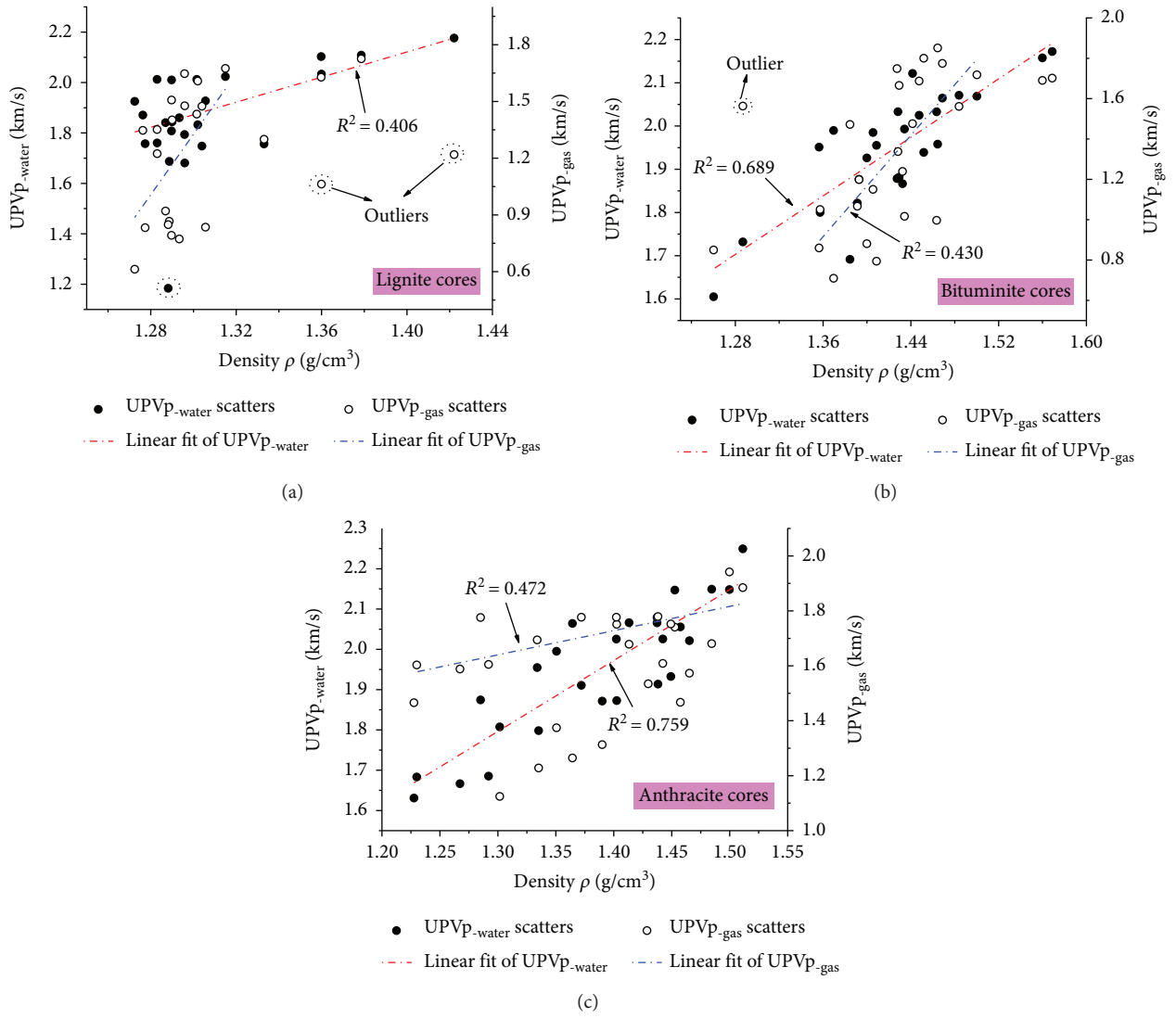

Figure 6: Scatterplot and distribution of velocity data and the corresponding trends between UPVp and density for (a) lignite, (b) bituminite, and (c) anthracite at water/gas-saturated conditions.

conditions, and as coal density increases, the UPVp velocity is different but generally trends upward. The values are listed in Table 5. The linear correlation coefficients for the anthracite UPVp values were 0.759 and 0.472, respectively, under water- and gas-saturated conditions, whereas the corresponding coefficients for bituminite coal were 0.689 and 0.430, respectively. For water-saturated lignite coal, the linear fitting coefficient was 0.406, and its $UPVp_{-gas}$ scatter had

Table 5: Correlations between UPVp and porosity under water and gas saturation.

	Condition	Equation	R^2
Lignite	Water saturation	$UPVp_{-water} = 2.49^{*}\rho - 1.36$	0.406
	Gas saturation	\	\
Bituminite	Water saturation	$UPVp_{-water} = 1.69^{*}\rho - 0.46$	0.689
	Gas saturation	$UPVp_{-gas} = 6.28^{*}\rho - 7.62$	0.430
Anthracite	Water saturation	$UPVp_{-water} = 1.76^{*}\rho - 0.49$	0.759
	Gas saturation	$UPVp_{-gas} = 0.88^{*}\rho + 0.49$	0.472

poor correlation with density (R^2 less than 0.20), which might be attributed to the low rank and complex crack properties due to the large anisotropy, causing high possibility of discrete velocity distribution.

It should be noticed that there were several outliers of UPVp scatter for lignite and bituminite due to their high dispersion, and these outliers were labeled using the dotted cycles. The fitting difference might be explained from three aspects: (a) the presence of complex components, such as grains with different sizes, mineral distribution, or incomplete evolution of the plant material in the coal, leads to greater anisotropy in the lignite coal matrix, resulting in random distributions of density and wave velocity [24, 36]. (b) Fluids may occupy the void space, increasing the whole saturated coal density. Given that the water density is larger than gas density, the water-saturated coal had larger UPV values than the gas-saturated coal [37, 38]. Different coals have various UPVp values, which are mostly affected by physicochemical properties and coal rank. (c) Different coals have various pore structures and distributions. For example, anthracite has a large volume of micropores, whereas lignite and bituminite have numerous macropores or cracks [48]. The occupied water in the smaller volume pores is more likely to promote an increase in velocity with increasing density.

4.4. Correlations between the UPVp Values and Porosity. The presence of fissures always has a significant impact on pulse wave transmission, and wave velocity increases parallel to the bedding planes, but decreases in the perpendicular direction [49–51]. In this paper, coal porosity φ was calculated using a weighing method described as follows:

$$\varphi = \frac{V_{crack}}{V_{core}} = \frac{\Delta M}{\rho_w V_{core}} = \frac{M_{water} - M_{pre}}{\rho_w V_{core}} = \frac{4\left(M_{water} - M_{pre}\right)}{\rho_w \pi D^2 h}, \tag{3}$$

where V_{crack} and V_{core} are the volumes (cm^3) of cracks and coal cores, respectively; ρ_w is the density of water and equals to 1.0 g/cm^3; ΔM is the mass difference between M_{water} and M_{pre}, (g); M_{water} and M_{pre} are the coal mass at completely saturated and dry conditions, respectively (g); and D and h are the diameter and height of the coal cores, respectively, (cm).

The porosity calculated in equation (3) only considers connected cracks, and closed pores are excluded for simplification. Figure 7 shows the scatterplot of data and the correlations between the UPVp and φ under water and gas saturation. The lignite cores had a mean φ value of 3.06, the bituminite cores had a mean φ value of 2.09, and the anthracite cores had a mean φ value of 1.21. This finding indicates that coal rank is inversely related to porosity; the coal with a lower rank had a larger porosity. For each kind of coal, the small porosity difference might be related to the number of connected cracks and the fact that some internal closed pores were not filled with water. However, the trend did not have disadvantageous impacts on the final results. The existence of fissures or cracks caused some reflection and refraction of waves at the crack surface, and some friction at grain boundaries, directly causing amplitude attenuation and a large energy decrease and delaying the first arrival time of the wave, finally resulting in a velocity decrease, which was coincident with the conclusion by Kohlhauser and Hellmich [51] and Li et al. [52].

As shown in Figure 7 and Table 6, the declining trends of lignite and bituminite under gas saturation were higher than under water saturation, whereas for anthracite, correlations between $UPVp_{-water}$ and φ had a larger decline compared to correlations between $UPVp_{-gas}$ and φ. The decline difference might be related to water sensitivity of the coals. That is, micropores within anthracite generally account for 50% of the total pores [53, 54], and water exhibits various modes of infiltration, such as seepage in macropores as well as diffusion and adsorption in micropores. Due to the larger adsorption capacity of anthracite, the adsorbed water molecules could squeeze into voids and increase the distance between grains, which might have some inverse impacts on the velocity. Meanwhile, the velocity of water-saturated cores decreased with increasing φ, which indicated that very large numbers of unconnected pores existed in addition to the pores filled with water. Crack properties such as surface physicochemistry, fracture roughness, and connectivity, should also be considered in the evaluation of velocity transmission.

4.5. Potential Applications. Based on the above results and the reported results from Kahraman [16], Vasanelli et al. [28], and Liu et al. [37], it is evident that wave velocity has some correlations with the rock properties, such as density and porosity. According to Chen et al. [21], Sansalone and Streett [55], and Bogas et al. [56], the coal regarded as a homogenous material simply might have some relations between velocity and the related mechanical parameters, shown in the following equation:

$$UPV = \sqrt{\frac{E_d}{\rho} \cdot \frac{(1 - \upsilon_d)}{(1 + \upsilon_d) \cdot (1 - 2\upsilon_d)}}, \tag{4}$$

$$\upsilon_d = \frac{1/2(UPVp/UPVs)^2 - 1}{(UPVp/UPVs)^2 - 1}, \tag{5}$$

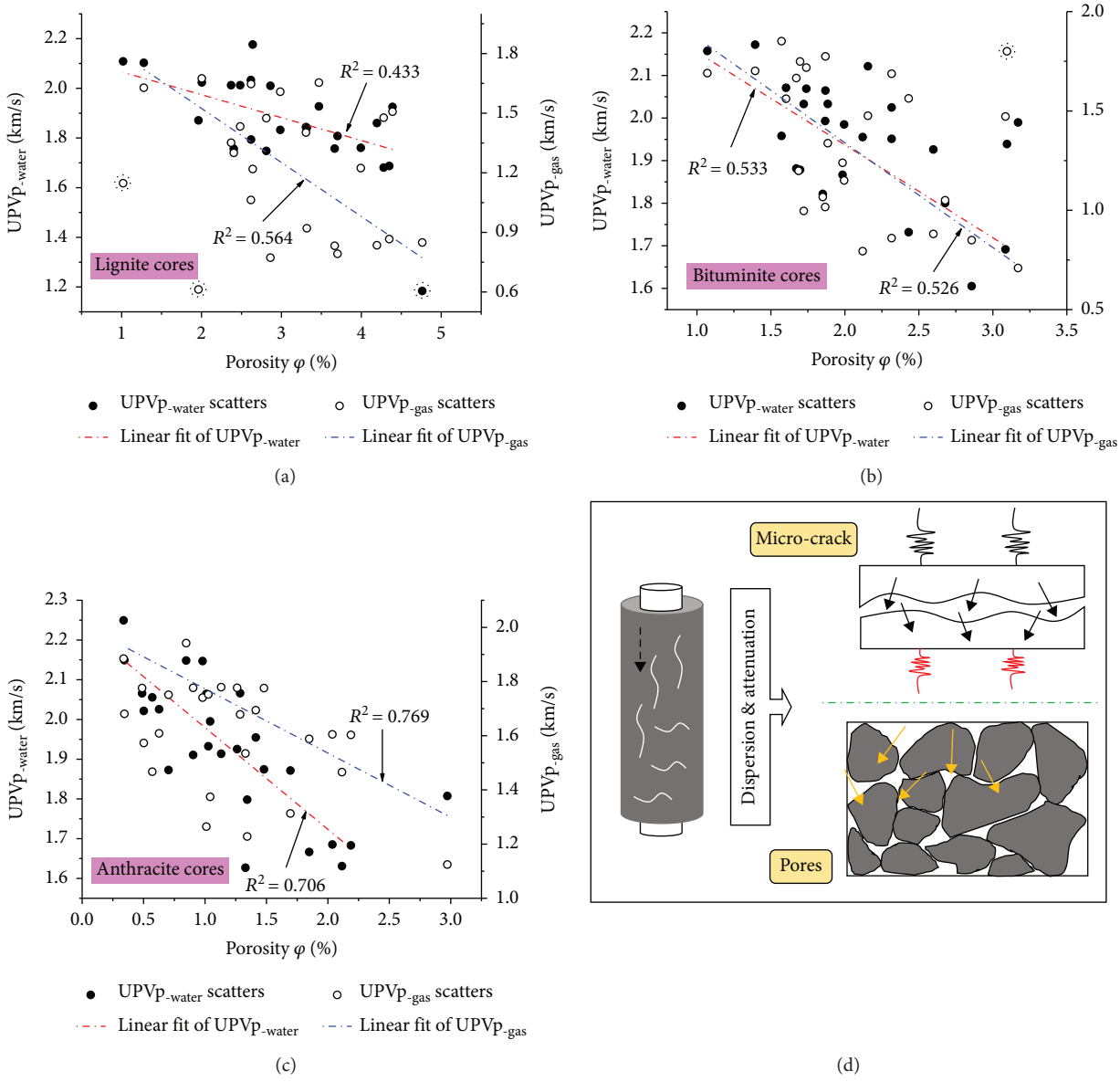

Figure 7: Scatterplot and linear correlations between UPVp and porosity under water and gas saturation for (a) lignite, (b) bituminite, and (c) anthracite (d) showing a sketch of wave transmission within the coal matrix.

Table 6: Linear fit equations between UPVp and porosity at water and gas saturation.

	Condition	Equation	R^2
Lignite	Water saturation	$UPVp_{-water} = -0.092^{*}\varphi + 2.16$	0.433
	Gas saturation	$UPVp_{-gas} = -0.272^{*}\varphi + 2.07$	0.564
Bituminite	Water saturation	$UPVp_{-water} = -0.218^{*}\varphi + 2.37$	0.533
	Gas saturation	$UPVp_{-gas} = -0.527^{*}\varphi + 2.39$	0.526
Anthracite	Water saturation	$UPVp_{-water} = -0.256^{*}\varphi + 2.24$	0.706
	Gas saturation	$UPVp_{-gas} = -0.237^{*}\varphi + 2.01$	0.769

where υ_d is the dynamic Poisson's ratio, E_d is the elastic modulus, and ρ is the density. Based on the above equation, the P-wave velocity is directly proportional to the square root of the dynamic modulus of elasticity and inversely proportional to the square root of its density, and the Poisson's ratio υ_d is proportional to the square of velocity ratio. Based on

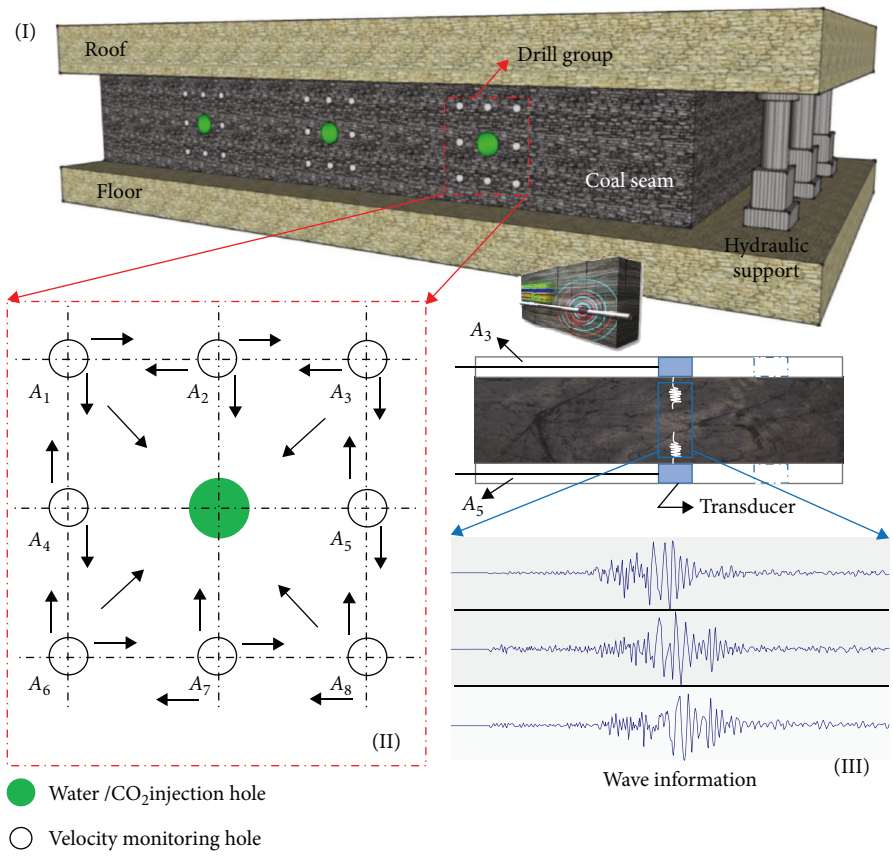

Figure 8: Potential application of velocity measurements by hydraulic fracturing or CO_2 fracturing during enhanced CBM recovery.

equations (4) and (5), the determined UPVp and UPVs could approximately deduce the elastic parameters, and the relevant intensity region of specified coal layers could be plotted, from which the potential fracture-generating region could be drawn. The UPV test method has application in enhanced CBM recovery by hydraulic fracturing or aqueous fracturing methods (such as CO_2 fracturing), as shown in Figure 8.

A number of drill groups are advanced into a coal seam with each group containing a single fracturing fluid (water or LCO_2) injection hole and eight monitoring holes ($A_1, A_2, \ldots, A_8$) around the injection hole (hole depth of J), as shown in parts (I) and (II) in Figure 8. Taking the example of monitoring holes A_3 and A_5, two transducers are initially placed at the bottom of the monitoring holes and simultaneously moved by the same distance (l) from the hole bottom in sequence to measure the velocity distributions of the region between hole A_3 and hole A_5, and velocity values are recorded as $V_{A3-A5(i)}$ ($i = 0,1,2, \ldots, J/l$). When the fracturing process is finished, the posttest velocity of the specific region is recorded as $V'_{A3-A5(i)}$ ($i = 0,1,2, \ldots, J/l$). By comparing the pre- and posttest velocities, the relationship between velocity and cracks can be deduced:

$$\begin{cases} V'_{A_3-A_5(i)} < V_{A_3-A_5(i)}\text{; some cracks are generated,} \\ V'_{A_3-A_5(i)} = V_{A_3-A_5(i)}\text{; no cracks are generated.} \end{cases} \quad (6)$$

Thus, it is possible to locate petrological changes caused by the mechanical effects of water or CO_2 injection, rapidly identify the effective fracture zone, and deduce fracture orientations. Depending on the collected velocity data, it is possible to forecast changes in physical parameters when subjected to crustal stress. This potential application could save a significant amount of core drilling work and help to obtain useful information about coal at depth in real time.

Although correlations among velocity, density, and porosity of water and gas-saturated coal cores have been identified, there is still a need for further study. For example, velocities recorded in different cores with various fluid media and fluid contents should be further investigated and velocity anisotropy should be quantified in future research. Additionally, correlations between velocities of different coal types under fluid saturation and the relevant elastic properties should be tested.

5. Conclusions

Based on this study, the following major conclusions can be drawn:

(i) The velocities recorded in the three different coal ranks displayed various distributions and discrete degrees, likely related to rank and saturation media. By comparing the range of the UPVp and UPVs box plots, it is evident that the UPVp is more accurate or

reliable for characterizing the existence of micro- or macrocracks with the assistance of adsorbed water

(ii) The UPVp values of lignite, bituminite, and anthracite coals showed positive linear correlations with their corresponding UPVs values, under water and gas saturation. The UPVp values correlated positively with the density of water/gas-saturated cores and correlated negatively with the porosity of both prepared cores

(iii) The ratio of UPVp/UPVs had a negative linear correlation with the UPVs values for lignite, bituminite, and anthracite, and the different decline trends might be attributed to coal rank. The coals with lower rank had large amounts of fissures. The larger difference of acoustic resistance between coal and gas dissipated a large amount of energy by means of wave reflection or refraction

Data Availability

The data used to support the findings of this study are available from the corresponding author upon request.

Conflicts of Interest

The authors declare that they have no conflicts of interest.

Acknowledgments

This work was financially supported by the National Key Technologies Research & Development program (2018YFC0808403), the National Natural Science Foundation of China (51774278), the Natural Science Foundation of Jiangsu Province (BK20170001), and the Jiangsu Province Fifth 333 High-Level Talents Training Project (BRA2018032).

Supplementary Materials

The total data in the paper are listed as the following table: parameter data of lignite cores under water/gas-saturated conditions, parameter data of bituminite cores under water/-gas-saturated conditions, and parameter data of anthracite cores under water/gas-saturated conditions. *(Supplementary Materials)*

References

[1] I. Palmer, "Coalbed methane completions: a world view," *International Journal of Coal Geology*, vol. 82, no. 3-4, pp. 184–195, 2010.

[2] N. Vedachalam, S. Srinivasalu, G. Rajendran, G. A. Ramadass, and M. A. Atmanand, "Review of unconventional hydrocarbon resources in major energy consuming countries and efforts in realizing natural gas hydrates as a future source of energy," *Journal of Natural Gas Science and Engineering*, vol. 26, pp. 163–175, 2015.

[3] P. Booth, H. Brown, J. Nemcik, and R. Ting, "Spatial context in the calculation of gas emissions for underground coal mines," *International Journal of Mining Science and Technology*, vol. 27, no. 5, pp. 787–794, 2017.

[4] J. Xu, C. Zhai, L. Qin, S. Wu, Y. Sun, and R. Dong, "Characteristics of pores under the influence of cyclic cryogenic liquid carbon dioxide using low-field nuclear magnetic resonance," *Geofluids*, vol. 2018, Article ID 1682125, 14 pages, 2018.

[5] Q. Zou and B. Lin, "Fluid–solid coupling characteristics of gas-bearing coal subjected to hydraulic slotting: an experimental investigation," *Energy & Fuels*, vol. 32, no. 2, pp. 1047–1060, 2018.

[6] G. Ni, Z. Li, and H. Xie, "The mechanism and relief method of the coal seam water blocking effect (WBE) based on the surfactants," *Powder Technology*, vol. 323, pp. 60–68, 2018.

[7] T. A. Moore, "Coalbed methane: a review," *International Journal of Coal Geology*, vol. 101, pp. 36–81, 2012.

[8] J. Xu, C. Zhai, and L. Qin, "Mechanism and application of pulse hydraulic fracturing in improving drainage of coalbed methane," *Journal of Natural Gas Science and Engineering*, vol. 40, pp. 79–90, 2017.

[9] T. Liu, B. Lin, Q. Zou, C. Zhu, and F. Yan, "Mechanical behaviors and failure processes of precracked specimens under uniaxial compression: a perspective from microscopic displacement patterns," *Tectonophysics*, vol. 672-673, pp. 104–120, 2016.

[10] Q. Li, B. Lin, and C. Zhai, "The effect of pulse frequency on the fracture extension during hydraulic fracturing," *Journal of Natural Gas Science and Engineering*, vol. 21, pp. 296–303, 2014.

[11] C. Zhai, J. Xu, S. Liu, and L. Qin, "Fracturing mechanism of coal-like rock specimens under the effect of non-explosive expansion," *International Journal of Rock Mechanics and Mining Sciences*, vol. 103, pp. 145–154, 2018.

[12] E. A. Novikov, R. O. Oshkin, V. L. Shkuratnik, S. A. Epshtein, and N. N. Dobryakova, "Application of thermally stimulated acoustic emission method to assess the thermal resistance and related properties of coals," *International Journal of Mining Science and Technology*, vol. 28, no. 2, pp. 243–249, 2018.

[13] J. Lazar, T. Kanduč, S. Jamnikar, F. Grassa, and S. Zavšek, "Distribution, composition and origin of coalbed gases in excavation fields from the Preloge and Pesje mining areas, Velenje Basin, Slovenia," *International Journal of Coal Geology*, vol. 131, pp. 363–377, 2014.

[14] L. D. Connell, S. Mazumder, R. Sander, M. Camilleri, Z. Pan, and D. Heryanto, "Laboratory characterisation of coal matrix shrinkage, cleat compressibility and the geomechanical properties determining reservoir permeability," *Fuel*, vol. 165, pp. 499–512, 2016.

[15] Q. Lyu, X. Long, P. G. Ranjith, J. Tan, Y. Kang, and W. Luo, "A damage constitutive model for the effects of CO_2-brine-rock interactions on the brittleness of a low-clay shale," *Geofluids*, vol. 2018, Article ID 7321961, 14 pages, 2018.

[16] S. Kahraman, "The correlations between the saturated and dry P-wave velocity of rocks," *Ultrasonics*, vol. 46, no. 4, pp. 341–348, 2007.

[17] O. Kılıç, "The influence of high temperatures on limestone P-wave velocity and Schmidt hammer strength," *International Journal of Rock Mechanics and Mining Sciences*, vol. 43, no. 6, pp. 980–986, 2006.

[18] R. Fort, M. Alvarez de Buergo, and E. M. Perez-Monserrat, "Non-destructive testing for the assessment of granite decay in heritage structures compared to quarry stone,"

International Journal of Rock Mechanics and Mining Sciences, vol. 61, pp. 296–305, 2013.

[19] M. Favaro, R. Mendichi, F. Ossola et al., "Evaluation of polymers for conservation treatments of outdoor exposed stone monuments. Part I: photo-oxidative weathering," *Polymer Degradation and Stability*, vol. 91, no. 12, pp. 3083–3096, 2006.

[20] M. Myrin and K. A. Malaga, "A case study on the evaluation of consolidation treatments of Gotland sandstone by use of ultrasound pulse velocity measurements," in *Heritage, Weathering and Conservation, vol. 2*, R. Fort, M. Alvarez de Buergo, M. Gomez-Heras, and C. Vazquez-Calvo, Eds., pp. 749–755, Taylor and Francis, London, UK, 2010.

[21] H. Chen, B. Jiang, T. Chen, S. Xu, and G. Zhu, "Experimental study on ultrasonic velocity and anisotropy of tectonically deformed coal," *International Journal of Coal Geology*, vol. 179, pp. 242–252, 2017.

[22] J. Vilhelm, V. Rudajev, T. Lokajíček, and R. Živor, "Velocity dispersion in fractured rocks in a wide frequency range," *Journal of Applied Geophysics*, vol. 90, pp. 138–146, 2013.

[23] K. Nakahata, G. Kawamura, T. Yano, and S. Hirose, "Three-dimensional numerical modeling of ultrasonic wave propagation in concrete and its experimental validation," *Construction and Building Materials*, vol. 78, pp. 217–223, 2015.

[24] E. Yasar and Y. Erdogan, "Correlating sound velocity with the density, compressive strength and Young's modulus of carbonate rocks," *International Journal of Rock Mechanics and Mining Sciences*, vol. 41, no. 5, pp. 871–875, 2004.

[25] S. Kahraman, "Evaluation of simple methods for assessing the uniaxial compressive strength of rock," *International Journal of Rock Mechanics and Mining Sciences*, vol. 38, no. 7, pp. 981–994, 2001.

[26] G. Vasconcelos, P. B. Lourenço, C. A. S. Alves, and J. Pamplona, "Ultrasonic evaluation of the physical and mechanical properties of granites," *Ultrasonics*, vol. 48, no. 5, pp. 453–466, 2008.

[27] A. A. E. Aliabdo and A. E. M. A. Elmoaty, "Reliability of using nondestructive tests to estimate compressive strength of building stones and bricks," *Alexandria Engineering Journal*, vol. 51, no. 3, pp. 193–203, 2012.

[28] E. Vasanelli, D. Colangiuli, A. Calia, M. Sileo, and M. A. Aiello, "Ultrasonic pulse velocity for the evaluation of physical and mechanical properties of a highly porous building limestone," *Ultrasonics*, vol. 60, pp. 33–40, 2015.

[29] G. Zandt and C. J. Ammon, "Continental crust composition constrained by measurements of crustal Poisson's ratio," *Nature*, vol. 374, no. 6518, pp. 152–154, 1995.

[30] N. I. Christensen, "Poisson's ratio and crustal seismology," *Journal of Geophysical Research: Solid Earth*, vol. 101, no. B2, pp. 3139–3156, 1996.

[31] S. Chevrot and R. D. Van der Hilst, "The Poisson ratio of the Australian crust: geological and geophysical implications," *Earth and Planetary Science Letters*, vol. 183, no. 1-2, pp. 121–132, 2000.

[32] S. Ji, Q. Wang, and M. H. Salisbury, "Composition and tectonic evolution of the Chinese continental crust constrained by Poisson's ratio," *Tectonophysics*, vol. 463, no. 1-4, pp. 15–30, 2009.

[33] Q. Wang, S. Ji, S. Sun, and D. Marcotte, "Correlations between compressional and shear wave velocities and corresponding Poisson's ratios for some common rocks and sulfide ores," *Tectonophysics*, vol. 469, no. 1-4, pp. 61–72, 2009.

[34] T. Lokajíček, V. Rudajev, R. D. Dwivedi, R. K. Goel, and A. Swarup, "Influence of thermal heating on elastic wave velocities in granulite," *International Journal of Rock Mechanics and Mining Sciences*, vol. 54, pp. 1–8, 2012.

[35] A. Morcote, G. Mavko, and M. Prasad, "Dynamic elastic properties of coal," *Geophysics*, vol. 75, no. 6, pp. E227–E234, 2010.

[36] F. Dirgantara, L. M. Batzle, and B. J. Curtis, "Maturity characterization and ultrasonic velocities of coals," in *SEG Technical Program Expanded Abstracts 2011*, p. 4424, San Antonio, TX, USA, 2011.

[37] J. Liu, D. Liu, Y. Cai, Q. Gan, and Y. Yao, "Effects of water saturation on P-wave propagation in fractured coals: an experimental perspective," *Journal of Applied Geophysics*, vol. 144, pp. 94–103, 2017.

[38] M. J. Lwin, "The effect of different gases on the ultrasonic response of coal," *Geophysics*, vol. 76, no. 5, pp. E155–E163, 2011.

[39] G. Q. Yu, C. Zhai, L. Qin, Z. Q. Tang, S. L. Wu, and J. Z. Xu, "Changes to coal pores by ultrasonic wave excitation of different powers," *Journal of China University of Mining & Technology*, vol. 47, pp. 264–270, 2018.

[40] G. T. Kuster and M. N. Toksoz, "Velocity and attenuation of seismic waves in two-phase media: part I. theoretical formulations," *Geophysics*, vol. 39, no. 5, pp. 587–606, 1974.

[41] J. Xu, C. Zhai, S. Liu, L. Qin, and S. Wu, "Pore variation of three different metamorphic coals by multiple freezing-thawing cycles of liquid CO_2 injection for coalbed methane recovery," *Fuel*, vol. 208, pp. 41–51, 2017.

[42] T. Mandal, J. M. Tinjum, and T. B. Edil, "Non-destructive testing of cementitiously stabilized materials using ultrasonic pulse velocity test," *Transportation Geotechnics*, vol. 6, pp. 97–107, 2016.

[43] N. A. el Sayed, H. Abuseda, and M. A. Kassab, "Acoustic wave velocity behavior for some Jurassic carbonate samples, north Sinai, Egypt," *Journal of African Earth Sciences*, vol. 111, pp. 14–25, 2015.

[44] M. A. Kassab and A. Weller, "Study on P-wave and S-wave velocity in dry and wet sandstones of Tushka region, Egypt," *Egyptian Journal of Petroleum*, vol. 24, no. 1, pp. 1–11, 2015.

[45] Y. M. Wang, Y. K. Miao, X. J. Meng, G. Q. Shen, and Y. C. Dong, "The calculation technique of physical transverse wave velocity curve for rock," *Petroleum Geology and Recovery Efficiency*, vol. 13, pp. 58–61, 2006.

[46] J. Wang, S. Wu, J. Geng, and P. Jaiswal, "Acoustic wave attenuation in the gas hydrate-bearing sediments of Well GC955H, Gulf of Mexico," *Marine Geophysical Research*, vol. 39, no. 4, pp. 509–522, 2018.

[47] B. Das and R. Chatterjee, "Well log data analysis for lithology and fluid identification in Krishna-Godavari Basin, India," *Arabian Journal of Geosciences*, vol. 11, no. 10, 2018.

[48] X. J. Xu, J. Liu, and L. Wang, "Influence of pore size distribution of different metamorphic grade of coal on adsorption constant," *Journal of China Coal Society*, vol. 38, pp. 294–300, 2013.

[49] W. Li and Y. Cho, "Combination of nonlinear ultrasonics and guided wave tomography for imaging the micro-defects," *Ultrasonics*, vol. 65, pp. 87–95, 2016.

[50] C. S. Vishnu, M. A. Mamtani, and A. Basu, "AMS, ultrasonic P-wave velocity and rock strength analysis in quartzites devoid of mesoscopic foliations – implications for rock mechanics studies," *Tectonophysics*, vol. 494, no. 3-4, pp. 191–200, 2010.

[51] C. Kohlhauser and C. Hellmich, "Ultrasonic contact pulse transmission for elastic wave velocity and stiffness determination: influence of specimen geometry and porosity," *Engineering Structures*, vol. 47, pp. 115–133, 2013.

[52] H. Li, B. Q. Lin, Y. D. Hong et al., "Effect of microwave irradiation on pore and fracture evolutions of coal," *Journal of China University of Mining & Technology*, vol. 46, pp. 1194–1201, 2017.

[53] Y. G. Wang, M. G. Li, B. B. Chen, and S. H. Dai, "Experimental study on ultrasonic wave characteristics of coal samples under dry and water saturated conditions," *Journal of China Coal Society*, vol. 40, pp. 2445–2450, 2015.

[54] J. Xu, C. Zhai, S. Liu, L. Qin, and R. Dong, "Investigation of temperature effects from LCO_2 with different cycle parameters on the coal pore variation based on infrared thermal imagery and low-field nuclear magnetic resonance," *Fuel*, vol. 215, pp. 528–540, 2018.

[55] M. Sansalone and W. B. Streett, *Impact-Echo Nondestructive Evaluation of Concrete and Masonry*, Bullbrier Press, Ithaca, NY, USA, 1997.

[56] J. A. Bogas, M. G. Gomes, and A. Gomes, "Compressive strength evaluation of structural lightweight concrete by nondestructive ultrasonic pulse velocity method," *Ultrasonics*, vol. 53, no. 5, pp. 962–972, 2013.